Comparison of heterogeneous and homogeneous bubble nucleation using molecular simulations

Brian R. Novak, Edward J. Maginn, and Mark J. McCready
Department of Chemical and Biomolecular Engineering, University of Notre Dame, Notre Dame, Indiana 46556, USA
(Received 15 January 2006; revised manuscript received 12 December 2006; published 8 February 2007)

NPT and $NP_{zz}T$ molecular dynamics simulations of Lennard-Jones atoms were used to compare homogeneous and heterogeneous nucleation. In the heterogeneous cases, the attraction between the fluid and a smooth fcc (100) surface was varied. Multiple simulations were used to determine nucleation times from which nucleation rates were estimated using a transient nucleation model. Calculations demonstrated a clear enhancement in nucleation rates in the heterogeneous cases compared to the homogeneous case. To obtain homogeneous nucleation rates similar to the heterogeneous cases required temperatures about 10 K higher. It was also found that void formation was favored as the attraction between the liquid and solid was decreased. Varying the system size, thermostatting method, and barostat time constant affected quantitative results, but not the qualitative trends.

DOI: 10.1103/PhysRevB.75.085413 PACS number(s): 68.35.Rh, 64.60.Qb, 64.70.Fx, 02.70.Ns

I. INTRODUCTION

Nucleation is a phenomenon that continues to be of both fundamental and practical interest. Efforts to improve the cooling rates of high performance CPU's, miniaturize direct methanol fuel cells, and produce perfect, spherical nanoscale particles all could be improved if a better understanding of the basic nucleation mechanisms could be achieved.

One particularly interesting issue concerns bubble nucleation in a superheated liquid near a solid surface. Classic theories for nucleate boiling invoke vapor trapped in the well of crevices or holes[1] with a pressure difference outside versus inside commensurate with the curvature imposed by the size of the crevice. Both laboratory studies[2,3] and household observations (e.g., water in a pot on your stove) are consistent with this mechanism. Typical length scales for the crevices are the order of a few to tens of microns with pressure differences less than one atm for water at 20 °C. The presumption of vapor trapped on a surface with *nanometer scale* defects, however, would theoretically require pressure differences of hundreds of atmospheres, something not supported by recent experiments. For example, Theofanous *et al.*[4] performed boiling experiments on clean surfaces with four nanometer mean surface roughness and found that superheats of only tens of K were required for nucleation compared with hundreds or thousands of K predicted by models. Clearly classic theories have limitations explaining nucleation on nearly smooth surfaces.

Atomistic simulations are an attractive means for studying phenomena on nanometer length scales, and there has been a good deal of work examining homogeneous bubble nucleation. Homogeneous nucleation rates have been computed in a Lennard-Jones system at negative pressure[5–7] and at positive pressure.[8,9] Homogeneous nucleation has also been studied in a varying mixture of monoatomic and diatomic Lennard-Jones oxygen,[10] and in unary and binary Lennard-Jones fluids.[11] Zahn[12] studied homogeneous nucleation in water at 100 °C using transition path sampling molecular dynamics.[13,14] The work of forming voids in a superheated Lennard-Jones fluid was calculated using umbrella sampling Monte Carlo simulations.[15,16] Corti and Debenedetti[17] studied the width of the transition region between nucleation and spinodal decomposition using restricted ensemble Monte Carlo simulations.

There have been fewer computational studies of heterogeneous systems. Maruyama and Kimura[18] studied bubble nucleation in a Lennard-Jones fluid between harmonic platinum walls. The nucleation was induced by moving the upper wall to reduce the pressure. The effect of surface wettability on contact angle was obtained by varying the platinum-fluid energy parameter. Yi *et al.*[19] studied the vaporization of a thin Lennard-Jones argon layer from a harmonic platinum wall. Explosive boiling on a hot surface of fluid with variable depth was studied using argon on a platinum surface[20] and using water on a gold surface.[21] Neimark and Vishnayakov[22] studied nucleation of a Lennard-Jones fluid in wetting spherical pores using Monte Carlo simulations.

The present work was undertaken to see if molecular scale behavior under phase-change conditions would reveal understandings that could be related to the larger scale phenomena that is observed with boiling experiments. Molecular dynamics simulations were utilized to investigate several fundamental aspects of bubble nucleation, including the differences between homogeneous and heterogeneous nucleation, how the nature of the fluid-solid interaction affects nucleation rates, and the structure and mechanism of formation of critical bubble nuclei during heterogeneous nucleation.

A. Simulation conditions

To examine the role surfaces play on nucleation, three heterogeneous systems having different solid-fluid interaction energies were studied. A homogeneous system was also investigated. The heterogeneous systems were simulated in the isothermal, isostress ($NP_{zz}T$) ensemble, while the homogeneous simulations were conducted in the isothermal, isobaric (NPT) ensemble. Nucleation was induced by rapidly increasing the fluid temperature to arrive at a metastable state point, after which the system was evolved in time until nucleation occurred. The fluid was modeled using the following 12–6 Lennard-Jones potential

TABLE I. Lennard-Jones parameters. The subscripts *ss*, *sf*, and *ff* are for solid-solid, solid-fluid, and fluid-fluid interactions, respectively.

	σ_{ff} (Å)	σ_{ss} (Å)	σ_{sf} (Å)	ϵ_{ff}/k_B (K)	ϵ_{ss}/k_B (K)	ϵ_{sf}/k_B (K)
Homogeneous	3.405			121.014		
Weak	3.405	3.405	3.405	121.014	1210.14	60.507
Neutral	3.405	3.405	3.405	121.014	1210.14	121.014
Strong	3.405	3.405	3.405	121.014	1210.14	191.340

$$\phi_{LJ}(r_{ij}) = 4\epsilon\left(\left(\frac{\sigma}{r_{ij}}\right)^{12} - \left(\frac{\sigma}{r_{ij}}\right)^{6}\right), \quad r_{ij} \leqslant r_c. \tag{1}$$

The potential and forces were truncated at $r_c = 11.9175$ Å, with long range corrections to the pressure and energy applied in the homogeneous case. The Lennard-Jones parameters were chosen to represent argon[7] and are given in Table I. The solid in the heterogeneous simulations was modeled as a 12–6 Lennard-Jones crystal having a starting lattice parameter of 5.405 Å and the (100) surface exposed to the fluid. During the simulations the solid retained its fcc character but was compressed slightly in the direction of the applied stress. Interaction parameters between the solid and fluid were varied to model a weakly attractive surface (small ϵ_{sf}), a neutral surface ($\epsilon_{sf} = \epsilon_{ff}$), and strongly attractive surface (large ϵ_{sf}). These different cases will subsequently be referred to as the weak, neutral, and strong cases. A listing of the solid potential parameters is given in Table I. For all the simulations, a time step of $\Delta t = 2.16$ fs was used.

1. Heterogeneous Simulations

For the heterogeneous cases, 2302 fluid atoms were simulated in contact with 648 solid atoms within a supercell consisting of $9 \times 9 \times 2$ unit cells. The configuration is shown in Fig. 1. Periodic boundary conditions were used in the x and y directions, while in the z direction mean field restraining wall potentials were used at the top and bottom of the cell. The position of the top wall potential was adjusted to maintain a constant normal stress (P_{zz}). The position of the bottom wall potential, which was placed below the solid atoms, was held constant to keep the solid in place. Note that the top wall potential only interacted with the fluid atoms and the bottom wall potential only interacted with the solid atoms. No truncation of the interactions was used; all of the atoms interacted with a wall potential at all times.

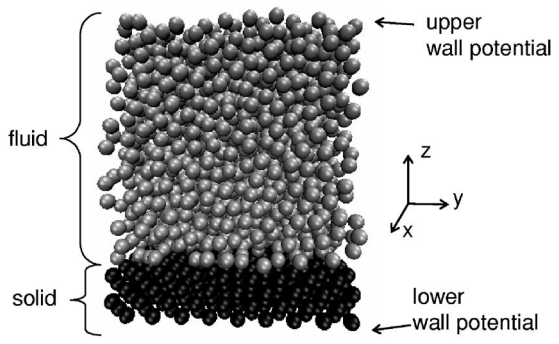

FIG. 1. The configuration of a heterogeneous simulation box. The light colored atoms are the fluid atoms and the dark colored ones are solid. The z directions were bounded by wall potentials, while periodic boundary conditions were used in the x and y directions. Image created using VMD.[23]

Interactions with the restraining walls were modeled using a 9-3 potential[24,25] in which the potential energy between a solid or fluid atom an absolute distance z from a wall is given by

$$\phi_{9-3} = \frac{2\pi\rho_w\sigma^3}{3}\epsilon\left[\frac{2}{15}\left(\frac{\sigma}{z+\Delta}\right)^9 - \left(\frac{\sigma}{z+\Delta}\right)^3\right],$$

$$\Delta = (2/5)^{1/6}\sigma. \tag{2}$$

The bottom wall was at $z = 0$ and the top wall was at the box height. The force on the top wall was $d\phi_{9-3}/dz$ while the force on the bottom wall was $-d\phi_{9-3}/dz$. This is a mean field potential and is based on integration of the 12–6 Lennard-Jones potential over the x (from $-\infty$ to ∞), y (from $-\infty$ to ∞), and z (from $-\infty$ to $-\Delta$) positions of wall atoms, approximated as a continuum with a wall number density, ρ_w. The density of the top wall was 2.25 times the density of the liquid at the initial temperature and pressure (96.0 K and 4.23 bar). The density of the bottom wall was 2.25 times the initial density of the solid. The Lennard-Jones parameters σ and ϵ in the wall potential were chosen to be the same as for the fluid-fluid and solid-solid interactions for the top and bottom wall, respectively.

To control the temperature of the system, a Nosé-Hoover thermostat was used, with a time constant of 0.05 ps. A single thermostat can be applied globally to all atoms in the system, or two separate thermostats can be used, one for the solid and one for the fluid. As discussed below, both approaches were used.

The normal stress at time step τ, $P_{zz}(\tau)$ was calculated as the sum of the forces per area on the upper wall and was controlled by changing the acceleration (a_w) of the upper wall using a proportional-integral controller with the integral evaluated using the trapezoid approximation

$$a_w(\tau) = k_P(P_{zz}(\tau) - P_{set}) + \frac{k_I\Delta t}{2}\sum_{i=1}^{\tau}[(P_{zz}(i) - P_{set}) + (P_{zz}(i-1) - P_{set})], \tag{3}$$

where P_{set} is the normal stress set point. The wall acceleration was controlled rather than the position for stability reasons. The values of k_P and k_I were 20.0 Å^2/amu and 0.005 Å^2/ps amu.

The wall position (r_w) and velocity (v_w) were advanced via a velocity Verlet type algorithm with a modified position move (Ref. 26),

$$r_w(\tau+1) = r_w(\tau) + \frac{\Delta t}{2}v_w(\tau) + \frac{3\Delta t^2}{4}a_w(\tau). \tag{4}$$

Because the system is metastable after ramping the temperature, any overshoot in the wall position leads to instabilities.

To control this, the wall velocity was throttled using the following approach. For the first 67 ps after ramping the temperature, integral control was not used in Eq. (3) and the maximum wall velocity was restricted using the following algorithm. A maximum initial wall velocity, v_{max}, of 0.9 Å/ps was set. If this value was exceeded during a time step, the wall velocity was assigned the maximum wall velocity and a new maximum wall velocity was set equal to $v_{max}+10^{-8}\tau$. After 67 ps, integral control was used in Eq. (3) and $v_{max}=10$ Å/ps

2. Homogeneous simulations

The homogeneous simulations were performed in the NPT ensemble using extended system dynamics[27] on 2500 atoms with full periodic boundary conditions. The thermostat time constant was 0.05 ps and the barostat time constant was 3.5 ps. As mentioned earlier, the usual long-range correction[26] to the pressure to account for the truncated forces was applied.

3. State points

A collection of N_0 stable, initial configurations were generated at 96.0 K and 4.23 bar for both the homogeneous and heterogeneous simulations by running equilibration simulations for a minimum of 648 ps (300 000 time steps). Once equilibrated, each system was rapidly brought to a metastable state by linearly ramping the Nosé-Hoover set point temperature to the desired value over a period of 1.67 ps. The global temperature reached the new set point temperature within 3 ps. Using an accurate equation of state,[28] the boiling point and spinodal temperature for the homogeneous system at this pressure were found to be 106.69 and 144.46 K, respectively. Note that for the homogeneous simulations it was necessary to use temperatures that were very near the spinodal line, given the fact that nucleation times are prohibitively long at lower temperatures. These temperatures are in the transition region between nucleate boiling and spinodal decomposition.[17] For the heterogeneous cases, the location of the spinodal is unknown and dependent on the nature of the solid-fluid interaction as well as the distance from the solid.[29]

4. Temperature and thermostatting method

While a single thermostat kept the overall temperature constant, the solid tended to heat up faster than the fluid when the set point temperature was increased. This caused the fluid to be at a lower overall temperature than the solid. Moreover, a temperature gradient was observed within the fluid phase. Figure 2 shows the overall solid and fluid temperatures for each heterogeneous case as a function of set point temperature. These temperatures were obtained by averaging over all runs in the time periods after ramping the temperature but before any phase change occurred. The weak system has the largest temperature difference between solid and fluid, and in all cases the difference increased with increasing set point temperature. The temperature difference between solid and fluid is small for the neutral and strong cases. Figure 3 shows the average temperature profile along

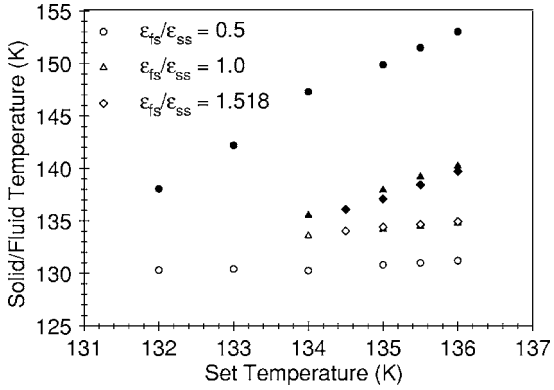

FIG. 2. Fluid and solid temperatures as a function of set point temperature for all heterogeneous cases. The open symbols are the fluid temperatures and the filled symbols of the same shape are the solid temperatures for each case.

the z direction for the weak case at 132.0 K for three separate simulations in which a single global thermostat was used. The temperature is nearly constant throughout the solid, which consists of the bottom four layers. This is indicative of the high thermal conductivity of this phase. The fluid adjacent to the solid is 5.0–8.0 K cooler than the solid, which is due to the heat transfer barrier that exists between the two phases. There is also a temperature gradient within the fluid itself. The differences in temperature between the solid and fluid as well as the fluid temperature gradients are all much smaller for the neutral and strong cases. To maintain both the fluid and solid temperatures at the set point temperature, two separate thermostats were used for the weak case simulations. Figure 4 shows that the use of dual thermostats maintains a nearly uniform temperature profile across both the solid and fluid, with fluctuations on the order of less than 1 K. Since the solid and fluid temperatures were very close to the set point temperature for the strong and neutral cases, only a single thermostat was used for those simulations. Obviously, two thermostats could be used for these cases as well to maintain even tighter temperature control. Finally we note that due to the presence of the mean field wall potentials, linear momentum in the direction nor-

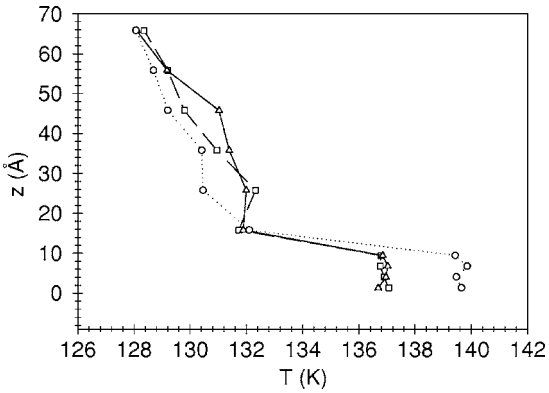

FIG. 3. Vertical temperature profiles for three independent weak case simulations at a global temperature of 132.0 K. The bottom four points are the solid layers and the others are the fluid. Lines are included to guide the eye.

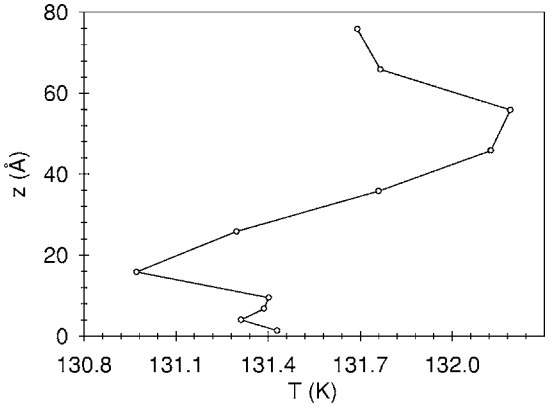

FIG. 4. Temperature as a function of z for the weak case averaged over 39 simulations at a set temperature of 132.0 K with dual thermostats. The bottom four points are the solid layers and the others are the fluid. Lines are included to guide the eye. Note the temperature scale differs from Fig. 3

mal to the surface was not conserved. When dual thermostats were used, linear momentum was not conserved in any direction. To remedy this, the linear momentum of the solid and fluid in the x and y directions were zeroed after each time step for the dual thermostat simulations. Table II lists all the simulation set point and fluid temperatures.

B. Nucleation times and rates

To determine nucleation rates with this simulation procedure, an objective measure is required for determining when a system actually nucleates. The nucleation times were estimated as the point in time when the fluid volume increase became significantly greater than the maximum volume fluctuations observed prior to the sharp increase in volume. The maximum volume fluctuations were greater in the homogeneous case than in the heterogeneous cases. For the heterogeneous case the nucleation times were found when the volume was 115% of the mean volume of the metastable state point, while for the homogeneous systems they were found at 130% of the mean volume. The average fluid volumes at the metastable state points were calculated using the average of the fluid volume from each simulation after reaching the metastable volume. Figure 5 shows a typical volume versus time plot for a homogeneous and weak heterogeneous simulation. The filled symbols designate the average volume of the system and the open symbols are the volumes where nucleation was assumed to occur. Changing the threshold volumes where nucleation is assumed to have occured does change the estimated nucleation rates somewhat, but the overall trends observed were not greatly impacted by these threshold values. To obtain nucleation rates, we consider that the N_0 different simulation boxes with volumes V_{box} are parts of a larger volume V.[30–33] When a nucleation event occurs in a simulation box, the volume available for nucleation decreases to V-V_{box}. The rate of change of the number of simulation boxes that have not yet nucleated (N) is given by

$$\frac{dN}{dt} = -J(t)NV_{\text{box}}, \tag{5}$$

where $J(t)$ is the nucleation rate at time t. Solving Eq. (5) in terms of t with the boundary condition that $N=N_0$ at the lag time t_0 and assuming a constant nucleation rate $J(t)=J_s$ and simulation box volume V_{box} gives a linear model with the following form:

$$t = -\ln\left(\frac{N}{N_0}\right) \Big/ (J_s V_{\text{box}}) + t_0. \tag{6}$$

Bartell[32] and Jacob and Bartell[33] used the method of moments[34] for transient nucleation to analyze crystallization simulations. They used an approximate inversion of the result to derive a nonlinear model in which the time for a nucleation event is given by

$$t = t_0 + \frac{g}{J_s V_{\text{box}}} - t_0\left(1 - \frac{0.5}{M_R^{2.5}}\right) \times \exp\left[-1.82\left(\frac{g}{J_s V_{\text{box}} t_0}\right)^{1/2} \Big/ (M_R - 1)^{0.41}\right],$$

$$g = -\ln\left(\frac{N}{N_0}\right). \tag{7}$$

This reduces to Eq. (6) if the reduced moment (M_R) is 1.0. A theoretical result by Kashchiev[35] agrees with the above expression for $M_R=1.4$. A recent analysis by Kashchiev[36] gave the dependence of M_R on critical nucleus size and supersaturation. We found that Eq. (7) represents the results of the present simulations better than does Eq. (6), and so it will be used in all subsequent analysis.

II. RESULTS

A. Fluid ordering

Due to the differing solid-fluid energy parameters in the heterogeneous cases, different levels of ordering of the fluid near the solid surface were observed. In all cases, there was some ordering. The density profiles at the initial state point are shown in Fig. 6. In the weak case, there was on average a larger low density region near the surface compared with the other cases. This made formation of voids near the weak surface easier, so nucleation occurred right at the fluid-solid interface for this case. In the neutral and strong cases, however, the fluid next to the surface was highly ordered and almost solidlike. In the strong case, the ordering extended further into the fluid than in the neutral case. For these two surface interactions, nucleation tended to occur *above* the solidlike fluid layers.

B. Nucleation times and rates

To estimate nucleation times and rates using Eq. (7), the following procedure was used. N_0 independent simulations were run at a given temperature. The time at which the volume reached the nucleation threshold value was recorded, after which time the simulation was stopped. A set of nucleation times was thus collected at each temperature and used in Eq. (7) to determine values of J_s and t_0, assuming $M_R=1.4$. The data were weighted according to the inverse square of the spacing between the points obtained from the

TABLE II. Steady state nucleation rates ($m^{-3}s^{-1}\times 10^{-35}$) and time lags ($ps\times 10^{-2}$) for all cases at each temperature for the nonlinear weighted fit. Estimated fluid temperatures (T_{fl}) as well as set point temperatures (T_{set}) are shown. They differ for the heterogeneous cases with one thermostat. Numbers in parentheses are the 68.3% confidence intervals. The number of simulations N_{sim} for each case is shown in the third column.

T_{set}(K)	T_{fl}(K)	N_{sim}	J_s	t_0
		Homogeneous		
143.5	143.5	39	0.016(0.0121, 0.0240)	9(7.1, 12.5)
143.7	143.7	32	0.04(0.026, 0.066)	1.0(0.75, 1.40)
144.0	144.0	44	0.12(0.089, 0.167)	1.1(0.90, 1.52)
144.5	144.5	43	1.1(0.85, 1.57)	1.6(1.27, 2.14)
		Weak		
132.0	130.30	39	0.25(0.182, 0.360)	6(4.3, 7.6)
133.0	130.41	38	0.6(0.44, 0.88)	4(3.4, 5.9)
134.0	130.25	40	4(2.7, 5.4)	6(5.0, 8.6)
135.0	130.82	40	7(5.0, 9.9)	6(4.9, 8.4)
135.5	131.00	37	8(5.9, 12.3)	6(4.6, 8.2)
136.0	131.21	40	5(3.5, 7.1)	5(3.7, 6.4)
		Neutral		
134.0	133.57	33	0.012(0.0081, 0.0192)	1.6(1.21, 2.24)
135.0	134.17	37	0.10(0.072, 0.149)	4(2.8, 5.0)
135.5	134.46	34	0.4(0.25, 0.54)	5(3.7, 6.8)
136.0	134.81	35	1.8(1.29, 2.70)	7(5.2, 9.4)
		Strong		
134.5	134.05	33	0.017(0.0116, 0.0276)	10(7.6, 14.0)
135.0	134.41	34	0.05(0.035, 0.076)	2.7(2.04, 3.71)
135.5	134.67	33	0.18(0.122, 0.291)	4(3.2, 6.0)
136.0	134.95	35	0.5(0.39, 0.83)	4(3.4, 6.2)
		Homogeneous, τ_b=0.1 ps		
144.0	144.0	107	0.23(0.197, 0.275)	0.7(0.57, 0.79)
144.5	144.5	107	1.2(1.06, 1.49)	0.54(0.461, 0.640)
		Weak, 2 Thermostat		
132.0	132.0	39	0.18(0.133, 0.264)	6(4.4, 7.6)
133.0	133.0	40	1.5(1.12, 2.23)	7(5.7, 9.8)
134.0	134.0	40	5.2(3.82, 7.63)	7(5.3, 9.1)
135.0	135.0	40	31(22.5, 45.0)	8(6.1, 10.6)
		Weak, 11×11 unit cells, 2 Thermostat		
132.0	132.0	38	0.13(0.094, 0.188)	5(3.6, 6.3)
		Weak, 13×13 unit cells, 2 Thermostat		
132.0	132.0	40	0.12(0.091, 0.182)	4(3.1, 5.3)
		Weak, 4604 fluid atoms, 2 Thermostat		
132.0	132.0		>0.19	

fit using an iterative process.[33] The point with the longest time was given zero weight. The weighting should provide a better estimate of the nucleation rate and lag time than a nonweighted fit, since the points at the longest times are the least accurate due to their low probability of occurrence. Note that the nucleation rate will depend on the value of M_R used in the fitting. As mentioned above, a value M_R=1.4 was assumed.[35] We note, however, that the qualitative trends in nucleation rates between the different cases are independent of the exact value of M_R. As an example of the type of fit achieved by the model, Fig. 7 shows plots of $-\ln(N/N_0)$ vs. nucleation time for the neutral case at three temperatures. The fits for the other cases are similar.

Table II shows the estimated nucleation rates and time lags obtained from fitting the simulation results to Eq. (7). The method used to determine errors in the parameters is described in the Appendix. The temperatures used in the homogeneous cases were about 10 K higher than those used in the heterogeneous cases to get nucleation rates that are in the same range. The nucleation rate decreased with increasingly attractive surfaces. There were no clear trends in the time lags with temperature or surface.

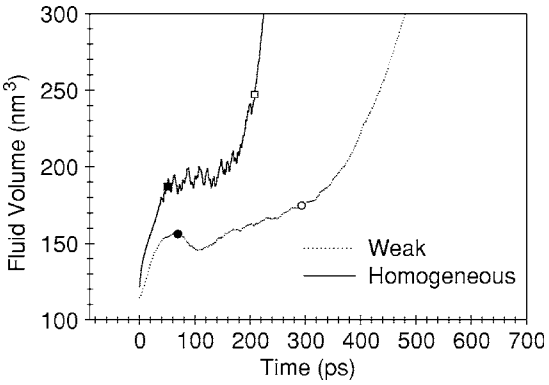

FIG. 5. Volume as a function of time for the weak and homogeneous cases. Open symbols are the points at the nucleation time. Filled symbols are the volumes used to calculate the average volume.

The differences in nucleation rates between the heterogeneous systems were correlated with the strength of interaction between the fluid and the solid, and consequently with the ordering near the nucleation site. Making the surface more attractive decreased the nucleation rates, but there was a limit to this. Once the interactions were strong enough to induce solidlike order of the fluid near the surface, further increasing the interaction energy had little effect on nucleation rates. Thus the strong and neutral surfaces had similar nucleation rates, while the weak case had much higher rates at the same temperature.

Changing the threshold volume used to determine the nucleation times in the heterogeneous cases from 15 to 30% above the average volume usually increased the nucleation rate. As shown in Table III, the average increase was 37.5% in the weak case. In the neutral case, the average increase was 26.1%, while in the strong case the average change was 9.3%. In the neutral and strong case the nucleation rate decreased for the lowest and two lowest temperatures, respectively. In these cases the increase in nucleation rate also became larger with increasing temperature.

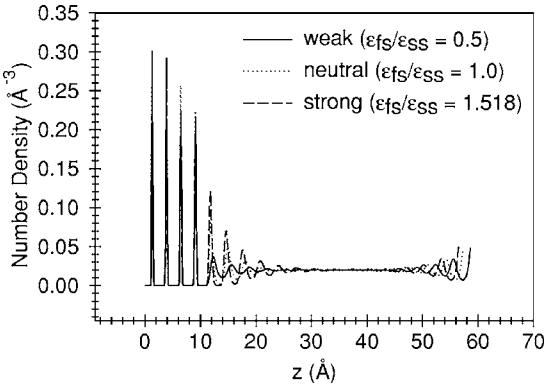

FIG. 6. Number density profiles for the three heterogeneous cases at the initial state point (96.0 K). The first four peaks are the solid layers and the other peaks are fluid. All three cases show some ordering near the solid surface. There is also some ordering at large z due to the top wall potential. The more attractive surfaces show more ordering and this ordering extends further into the liquid.

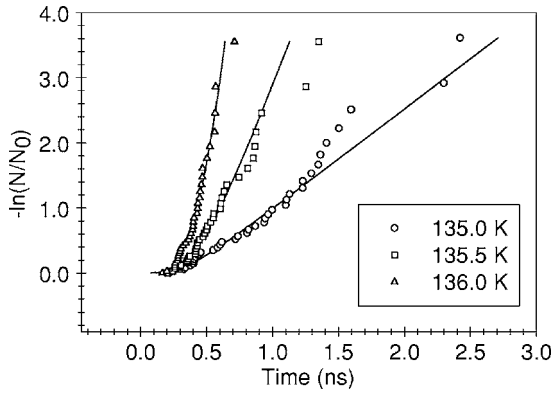

FIG. 7. Nucleation times vs the negative logarithm of the ratio of the number of nonnucleated simulations to the total number of simulations. The symbols are simulation results for the neutral case and lines are the fit to Eq. (7). The temperatures in the legend are the set point temperatures.

When controlling the temperature of the solid and fluid separately, nucleation rates increased by up to a factor of four with the largest difference at the highest temperature. This was probably due to the increasing difference in fluid temperature compared to set point temperature as seen in Fig. 2. Time lags t_0 were essentially unchanged. The net result was that, while differences in thermostatting method did affect the actual values obtained for the nucleation rate, it did not appear to qualitatively change the basic finding that *the presence of even a smooth surface with no solid or fluid impurities greatly enhances nucleation rates when compared*

TABLE III. Comparison of steady state nucleation rates ($m^{-3}s^{-1}\times 10^{-35}$) for the one thermostat heterogeneous cases when the nucleation times were at 1.15 times the average volume or 1.3 times the average volume. Estimated fluid temperatures (T_{fl}) as well as set point temperatures (T_{set}) are shown. Numbers in parentheses are the 68.3% confidence intervals.

T_{set}(K)	T_{fl}(K)	J_s(1.15)	J_s(1.3)
		Weak	
132.0	130.30	0.25(0.182, 0.360)	0.29(0.218,0.431)
133.0	130.41	0.6(0.44, 0.88)	0.9(0.67,1.3)
134.0	130.25	4(2.7, 5.4)	5(3.7,7.0)
135.0	130.82	7(5.0, 9.9)	9(6.4,12)
135.5	131.00	8(5.9, 12.3)	10(7.38,15.1)
136.0	131.21	5(3.5, 7.1)	7(5.6,11)
		Neutral	
134.0	133.57	0.012(0.0081, 0.0192)	0.012(0.0082,0.0180)
135.0	134.17	0.10(0.072, 0.149)	0.10(0.0726,0.149)
135.5	134.46	0.4(0.25, 0.54)	0.6(0.40,0.88)
136.0	134.81	1.8(1.29, 2.70)	2.5(1.79,3.90)
		Strong	
134.5	134.05	0.017(0.0116, 0.0276)	0.016(0.0116,0.0255)
135.0	134.41	0.05(0.035, 0.076)	0.05(0.035,0.073)
135.5	134.67	0.18(0.122, 0.291)	0.19(0.135,0.295)
136.0	134.95	0.5(0.39, 0.83)	0.7(0.49,1.1)

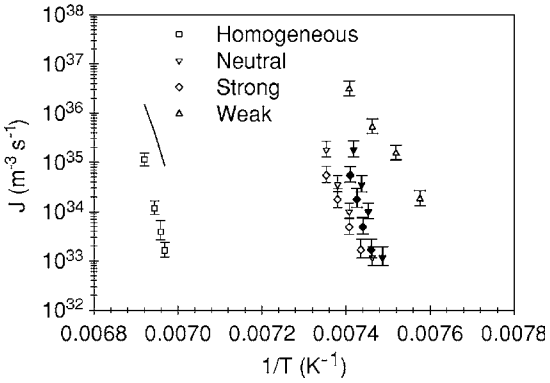

FIG. 8. Steady state nucleation rate J_s vs $1/T$ for all cases. Error bars are the 68.3% confidence intervals. The weak case data shown are for two thermostats. For the neutral and strong cases, the solid symbols are using the fluid temperature instead of set point temperature (open symbols). The line is the classical nucleation theory result for the same temperatures as the homogeneous case.

to homogeneous nucleation. Furthermore, the *weakly attractive surface induces nucleation much more readily than a neutral or strongly attractive surface*.

C. Temperature dependence of nucleation rate and comparison to classical nucleation theory

The nucleation rate as a function of inverse temperature is plotted in Fig. 8 for all cases. The solid and fluid were independently thermostatted for the weak case. For the strong and neutral cases, nucleation rates are shown using both the set point and fluid temparatures.

Nucleation is an activated process, so the steady state nucleation rate should be related to the free energy change for nucleation via an Arrhenius-type expression,

$$\ln(J_s) = \ln(A) - \frac{\Delta G}{k_B T}. \tag{8}$$

Although the data in Fig. 8 appear to be reasonably linear, both the pre-exponential factor (A) and free energy change (ΔG) are functions of temperature. For this reason, it was not possible to estimate reasonable free energy activation barriers. However, it is possible to compare the homogeneous simulation results with classical nucleation theory. The classical theory gives the nucleation rate for a superheated single component system as follows:[37]

$$J_s = \rho_l \left(\frac{3\gamma_{lv}}{\pi m}\right)^{1/2} \exp\left[\frac{-16\pi\gamma_{lv}{}^3}{3k_B T_l(\eta P_{\text{sat}} - P_l)^2}\right],$$

$$\eta = \exp\left[\frac{P_l - P_{\text{sat}}}{\rho_l k_B T_l}\right]. \tag{9}$$

The nucleation rate depends on the number density of the liquid (ρ_l), liquid-vapor surface tension (γ_{lv}), mass of a molecule (m), temperature (T_l), saturation pressure (P_{sat}), and liquid pressure (P_l). The saturation pressure was calculated using the Lennard-Jones equation of state.[28] The following experimental correlation for the temperature dependence of the liquid-vapor surface tension for argon was used (Ref. 38),

$$\gamma_{lv} = 3.823 \times 10^{-2}\left(1 - \frac{T}{T_c}\right)^{1.2927},$$

$$T_c = 158.9\text{K}, \tag{10}$$

where T_c is the Lennard-Jones critical temperature used by Johnson *et al.*[28] The number density of the liquid was calculated from the volumes obtained from the simulations. The free energy change is given by

$$\Delta G = \frac{16\pi\gamma_{lv}^3}{3(\eta P_{\text{sat}} - P_l)^2}, \tag{11}$$

and the critical radius is

$$r_{\text{crit}} = \frac{2\gamma_{lv}}{\eta P_{\text{sat}} - P_l}. \tag{12}$$

Using Eqs. (9) and (11), the nucleation rates and free energies were calculated at the temperatures used in the simulations.

TABLE IV. Free energies (kJ/mol nuclei), pre-exponential factors ($m^{-3}s^{-1}$) and steady state nucleation rates ($m^{-3}s^{-1} \times 10^{-35}$) from the classical theory at the temperatures used in the homogeneous case.

	Temperature (K)			
	143.5	143.7	144.0	144.5
ΔG	12.11	11.35	10.25	8.6535
$\ln A$	90.59	90.56	90.55	90.50
J_s	0.8584	1.605	4.036	15.00

The classical homogeneous nucleation rates, free energy changes, and pre-exponential factors obtained from Eq. (9) are shown in Table IV and plotted in Fig. 8. The classical nucleation rates were an order of magnitude *greater* than the simulated nucleation rates given in Table II. Previous simulation results have been compared to the classical theory and predicted nucleation rates that were 17 orders of magnitude higher,[6] three to four orders of magnitude higher,[7] and eight orders of magnitude lower[5] than the classical results. Zeng and Oxtoby[39] calculated nucleation rates using density functional theory and found they were at least ten orders of magnitude higher than the classical theory. Shen and Debenedetti[16] calculated free energy changes and found that the classical free energy change was increasingly larger than the simulated one with increasing temperature, meaning that the classical nucleation rates decrease too rapidly with increasing temperature. The size dependence of the surface tension should lead to an underestimate of nucleation rates by the classical theory.[40] The fact that our results matched the classical theory results better than those mentioned above is probably due to the surface tension and state point we used. Without data at other state points and a better estimation of surface tension, no general conclusion about the accuracy of the classical theory can be derived from this work.

D. Critical size

To characterize the size and structure of voids in the fluid, the simulation box was divided into small cubes of about 1.0 Å on a side. Cubes were designated as "empty" if their center was greater than 1.2σ from any atom center of mass.[18] To find the voids, the connectivity of these empty cubes was determined via a clustering algorithm similar to the one developed by Sevick *et al.*,[41] with the criterion that cubes were connected if they shared any point(s). This meant that the maximum number of other cubes that any cube was directly connected to was 26. This method only finds an approximate bubble volume. It will underestimate the volume if there are atoms enclosed by the empty cubes, since their volume is not counted.

To gain an understanding of the size of a critical nucleus, transition states for the weak case at 132.0 K, the neutral case at 134.0 K, the strong case at 134.5 K, and the homogeneous case at 143.5 K were found in the following manner. During a nucleation simulation a collection of configurations at various times near the nucleation event was recorded. Each of these configurations served as a starting point for twenty to forty new simulations in which the velocities were reset to random values chosen from a Maxwell-Boltzmann distribution. These simulations were then run for 216 ps for heterogeneous cases and 108 ps for the homogeneous case. The fraction of the simulations that nucleated was recorded. The starting configuration that resulted in roughly half of the simulations increasing in volume due to bubble nucleus growth was considered to be a transition state. The largest void was found in this configuration using the clustering algorithm and its volume was designated as the critical nucleus volume. The approximate critical volumes found were 1968 $Å^3$ for the weak case, 1594 $Å^3$ for the neutral case, 1117 $Å^3$ for the strong case, and 1647 $Å^3$ for the homogeneous case. The homogeneous critical volume using the radius from Eq. (12) and assuming a spherical nucleus is 1205 $Å^3$.

This method of computing transition states only gives an estimate of the critical nuclei volumes. For some cases, it was observed that some initial configurations having relatively small void volumes that were relatively spherical resulted in a larger fraction of nucleation events than others having larger void volumes with nonspherical shapes. This suggests that the proper reaction coordinate for liquid-vapor phase change may involve not only the size of the void, but also its shape.

Visualizations of the critical nuclei are shown in Fig. 9. The nuclei are clearly nonspherical. This is expected since the state points used are so near the spinodal. For the strong and neutral cases, the critical nucleus occurred above the ordered fluid layer, several atomic diameters above the solid surface. The ordered fluid remained in contact with the surface throughout the nucleation event. In the weak case, however, the critical nucleus formed right at the solid surface. This is in qualitative agreement with the findings of Carey and Wemhoff,[29] which suggested that nucleation occurs away from attractive walls due to a higher spinodal temperature near the wall.

E. Parameters affecting nucleation rates

To assess the impact various simulation parameters had on the results, the volume response as well as overall system size were varied to see how nucleation rates changed.

1. Volume response and barostat time constant

The barostat time constant for the homogeneous case was chosen to match as closely as possible the volume response observed in the heterogeneous simulations. As an example, Fig. 10 shows the volume response for the homogeneous and weak cases for a starting temperature of 96.0 K and an ending temperature of 132.0 K. The set point temperature was ramped up as discussed previously. The main difference is that the pressure was controlled via an extended system type barostat in the homogeneous case, while the acceleration of the top wall was used to control normal stress in the heterogeneous case. The responses were of course different, but the time taken to reach the new higher volume was about the same in each case. To test the role of the volume response dynamics on nucleation rates, another set of homogeneous simulations were carried out with a smaller barostat time constant of 0.1 ps compared with 3.5 ps originally. In addition, the temperature increase was a step function. The nucleation rates are shown in Table II.

Changing the volume response did lead to differences in homogeneous nucleation rates and time lags. The nucleation rate was larger for both of the common temperatures, 144.0 and 144.5 K, when the smaller barostat time constant was used. It was nearly twice as large at 144.0 K and about 9% larger at 144.5 K. On the other hand, the time lags were smaller for the smaller barostat time constant. Most of this latter result was due to the fact that a short temperature ramp was used in the original (large time constant) case instead of a step function. The primary effect of changing the form of the temperature change should be to just change the time lag, not the spacing of the nucleation events.

2. Simulation box size dependence

The dependence of the nucleation rate on system size was investigated for the homogeneous and the weak heterogeneous systems. For the homogeneous case, a set of simulations were run at 144.0 K with 5000 atoms, twice the number of the original simulations. For the weak case with dual thermostats at 132.0 K, sets of simulations were run in which the solid area was increased from 9×9 unit cells to 11×11 and 13×13 unit cells and a set of simulations for the 9×9 case were also run with twice the number of fluid atoms, thereby doubling the height of the fluid above the surface.

Doubling the size of the homogeneous system decreased the nucleation rate by about a factor of 5.5. For the heterogeneous case, increasing the solid area from 9×9 to 13×13 also decreased the nucleation rate by a factor of about 1.5. On the one hand, increasing the height of the fluid above the surface led to a decrease in the time for nucleation. At the lowest temperature simulated in the original case, the nucleation events occurred so rapidly that accurate estimates of the rates were not possible. Apparently, the larger fluid vol-

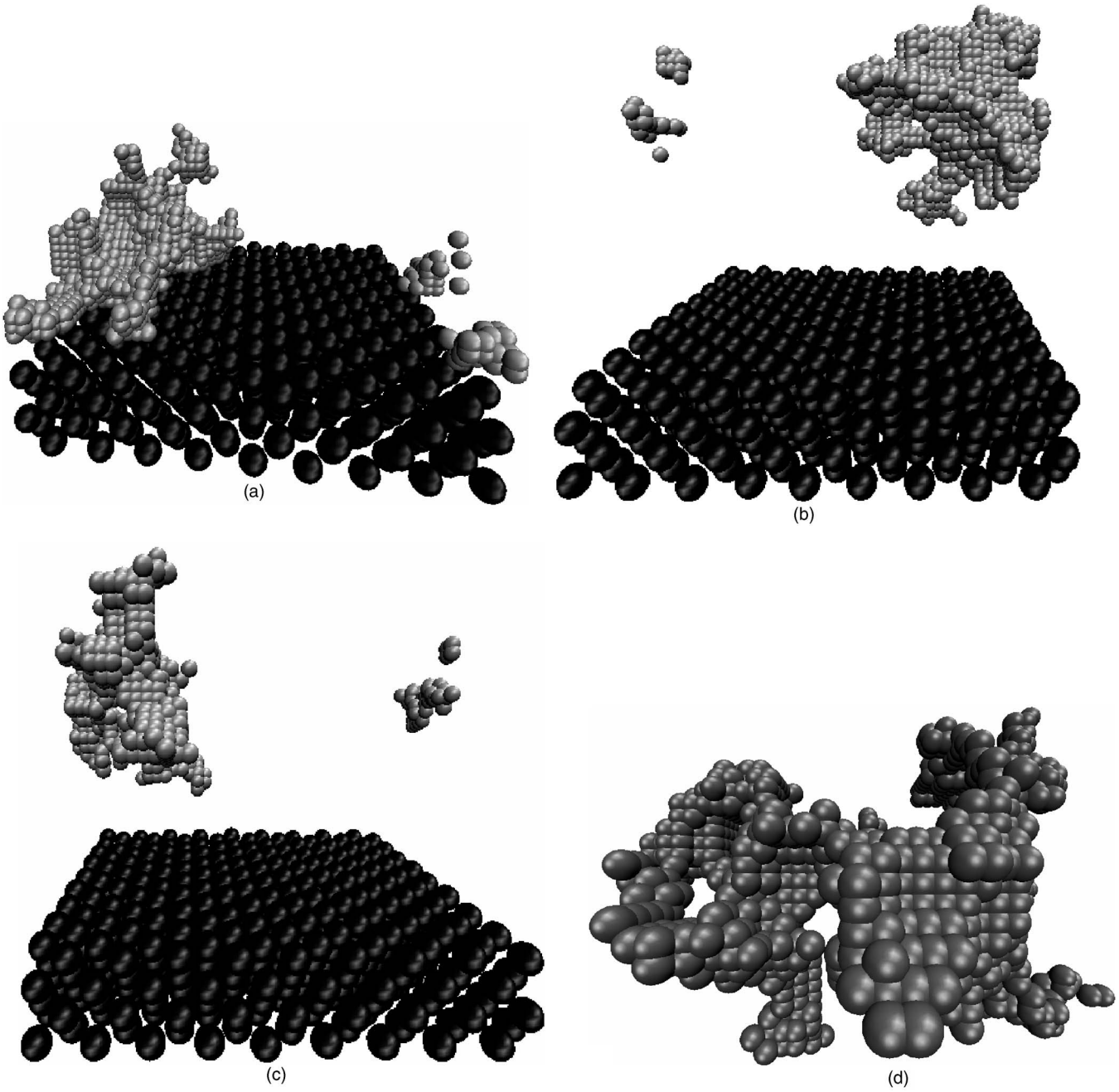

FIG. 9. Snapshots of critical voids. The sizes are 1968 Å^3, 1594 Å^3, 1117 Å^3, and 1647 Å^3 for the weak case at 132.0 K (a), the neutral case at 134.0 K (b), the strong case at 134.5 K (c), and the homogeneous case at 143.5 K (d), respectively. The silver spheres are voids and the black spheres are solid atoms. The liquid atoms are not shown. The small fragments to one side in the heterogeneous cases are a continuation of the void from the other side due to the periodic boundary conditions. Image created using VMD.[23]

ume above the surface enabled multiple nucleation events to occur. In any case, the trend of an enhanced nucleation rate due to the presence of a solid surface was observed regardless of system size. These results are summarized in Table II.

Increasing the box height by increasing the number of fluid atoms in the heterogeneous case lead to a larger nucleation rate, but the actual rate could not be computed because the volume increased so rapidly that getting an accurate volume of the metastable liquid was not possible at 132.0 K. Instead of one bubble forming near the surface, there appeared to be another one above it separated by a layer of liquid. This was seen in all five of the simulations that were visualized. The system size results are shown in Table II.

III. CONCLUSIONS

Homogeneous and heterogeneous bubble nucleation of an atomic 12–6 Lennard-Jones fluid was studied using molecular dynamics simulations. It was observed that nucleation rates were higher in the presence of an atomically smooth surface when compared to homogeneous nucleation. The homogeneous systems required temperatures about 10 K higher

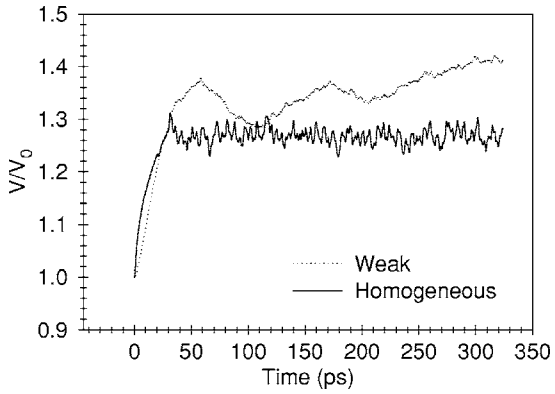

FIG. 10. Volume response after ramping the temperature from 96.0 to 132.0 K for one simulation each of the weak and homogeneous cases. The volume is reduced by its first saved value.

than the heterogeneous to get comparable nucleation rates. Among the different heterogeneous systems, it was observed that nucleation was fastest when the fluid was weakly attracted to the surface. In this case, nucleation occured near the surface. When the interaction energy between solid and fluid atoms increases, a solidlike adsorbed surface layer is formed, and nucleation occurs above this fluid layer.

Simulation parameters such as the barostat time constant and overall system size were varied to assess their role in the nucleation rates. It was found that nucleation rates do depend on the choice of these parameters, but that qualitative trends are insensitive to simulation details.

ACKNOWLEDGMENTS

This work was partially supported by the U.S. Army CECOM RDEC through agreement No. DAAB07-03-3-K414. Such support does not constitute endorsement by the U.S. Army of the views expressed in this publication. It was also partially supported through funding from the Indiana 21st Century Technology and Research Fund.

APPENDIX: ERRORS IN NUCLEATION RATES AND TIME LAGS

The method used by Jacob and Bartell[33] was used to calculate the errors in the nucleation rates and time lags. First, a large set of nucleation times (t_k) were generated by solving

$$KS(t_k) = h_k = -\ln([N_B - (k - 1 + f_B)]/N_B), \qquad (A.1)$$

$$S(t_k) = t_k\left(1 - \frac{1}{2}\,erfc\left[\frac{\ln(t_k/t_0) - a}{\sqrt{2b^2}}\right]\right) - t_0\left(1 - \frac{1}{2}\,erfc\left[\frac{\ln(t_k/t_0) - a}{\sqrt{2b^2}}\right]\right),$$

$$a = -\frac{1}{2}\ln(M_R),$$

$$b^2 = \ln(M_R).$$

K is the product of nucleation rate and volume (J_sV). The value of the fraction (f_B) of the width of the time bins (k) from which the times were chosen was 0.5. The number of times generated (N_B) was 10 000. The values of K and t_0 input were 1.0. The solution of Eqs. (A.1) was accomplished by using a small number as the initial guess for t_1 and the previous time as the initial guess for the other times. The solutions were found using the FindRoot function in MATHEMATICA 5.1.

Then 10 000 sets of N_0 times were chosen randomly from this set and K and t_0 were regressed from each set. From the variation in the parameters, an estimate of the errors from a single set of N_0 times was obtained. It was assumed that this is a reasonable estimate of the error for the one set of molecular dynamics simulations that was used for each case at each temperature.

The nucleation rates and time lags were approximately logarithm normally distributed. The probability for the logarithm normal distribution is

$$P(x) = \frac{1}{S\sqrt{2\pi x}}\exp\left[\frac{-(\ln(x) - M)^2}{2S^2}\right]. \qquad (A.2)$$

The parameters S and M are related to the standard deviation (σ) and mean (μ) of x through

$$S = \sqrt{\ln\left[\frac{\sigma^2}{\mu^2} + 1\right]},$$

$$M = \ln(\mu) - \frac{1}{2}\ln\left[\frac{\sigma^2}{\mu^2} + 1\right]. \qquad (A.3)$$

Using Eqs. (A.3) and the means and standard deviations, S and M were calculated for each N_0. Confidence intervals were calculated using

$$\frac{f}{2} = \int_a^\mu P(x)dx,$$

$$\frac{f}{2} = \int_\mu^b P(x)dx, \qquad (A.4)$$

where $0 < f < 1$ and a and b are the lower and upper bounds depending on f. For symmetric distributions $\mu - a = b - \mu$, but in general $\mu - a \neq b - \mu$. For the logarithm normal distribution $b - \mu > \mu - a$. For the normal distribution $f = erf(1/\sqrt{2}) \approx 0.683$ corresponds to intervals one standard deviation from the mean. This value of f was used in Eqs. (A.4) to find a and b.

To get the error for K and t_0 for a molecular dynamics data set, Eqs. (A.5) were used:

$$(\mu - a)_{\mathrm{MD}} = \left(\frac{y_{\mathrm{MD,ls}}}{y_{\mathrm{stoch,ls}}}\right)(\mu - a)_{\mathrm{stoch}},$$

$$(b - \mu)_{\mathrm{MD}} = \left(\frac{y_{\mathrm{MD,ls}}}{y_{\mathrm{stoch,ls}}}\right)(b - \mu)_{\mathrm{stoch}},$$

$$\sigma_{\mathrm{MD}} = \left(\frac{y_{\mathrm{MD,ls}}}{y_{\mathrm{stoch,ls}}} \right) \sigma_{stoch}. \tag{A.5}$$

In these equations, MD stands for molecular dynamics, ls for least squares, and stoch for stochastically generated using the procedure described in this section. The variable y is either K or t_0. These equations were tested by inputting different values of K or t_0 into Eqs. (A.1) and calculating the difference in the width of the intervals and standard deviation. To get the error in the nucleation rate, the random error in the volume was also considered, but was much smaller than the error in K.

[1] S. F. Jones, G. M. Evans, and K. P. Galvin, Adv. Colloid Interface Sci. **80**, 27 (1999).
[2] R. B. Dean, J. Appl. Phys. **15**, 446 (1944).
[3] E. N. Harvey, W. D. McElroy, and A. H. Whiteley, J. Appl. Phys. **18**, 162 (1947).
[4] T. G. Theofanous, J. P. Tu, A. T. Dinh, and T. N. Dinh, Exp. Therm. Fluid Sci. **26**, 775 (2002).
[5] T. Kinjo and M. Matsumoto, Fluid Phase Equilib. **144**, 343 (1998).
[6] T. Kinjo, K. Ohguchi, K. Yasuoka, and M. Matsumoto, Comput. Mater. Sci. **14**, 138 (1999).
[7] Y. W. Wu and C. Pan, Microscale Thermophys. Eng. **7**, 137 (2003).
[8] B. J. Garrison, T. E. Itina, and L. V. Zhigilei, Phys. Rev. E **68**, 041501 (2003).
[9] H. Okumura and N. Ito, Phys. Rev. E **67**, 045301(R) (2003).
[10] T. Tokumasu, K. Kamijo, M. Oike, and Y. Matsumoto, in *Fourth International Symposium on Cavitation* (California Institute of Technology, Pasadena, CA2001), p. SessionA1.005, http://cav2001.library.caltech.edu/388/00/tokumasu.pdf.
[11] S. Park, J.-G. Weng, and C.-L. Tien, Microscale Thermophys. Eng. **4**, 161 (2000).
[12] D. Zahn, Phys. Rev. Lett. **93**, 227801 (2004).
[13] P. G. Bolhuis, C. Dellago, and D. Chandler, Faraday Discuss. **110**, 421 (1998).
[14] C. Dellago, P. G. Bolhuis, F. S. Csajka, and D. Chandler, J. Chem. Phys. **108**, 1964 (1998).
[15] S. Punnathanam and D. S. Corti, Phys. Rev. E **69**, 036105 (2004).
[16] V. K. Shen and P. G. Debenedetti, J. Chem. Phys. **111**, 3581 (1999).
[17] D. S. Corti and P. G. Debenedetti, Chem. Eng. Sci. **49**, 2717 (1994).
[18] S. Maruyama and T. Kimura, Heat Technol. **18**, 69 (2000).
[19] P. Yi, D. Poulikakos, J. Walther, and G. Yadigaroglu, Int. J. Heat Mass Transfer **45**, 2087 (2002).
[20] X. Gu and H. M. Urbassek, Appl. Phys. B **81**, 675 (2005).
[21] Y. Dou, L. V. Zhigilei, N. Winograd, and B. J. Garrison, J. Phys. Chem. **105**, 2748 (2001).
[22] A. V. Neimark and A. Vishnyakov, J. Chem. Phys. **122**, 054707 (2005).
[23] W. Humphrey, A. Dalke, and K. Schulten, J. Mol. Graphics **14**, 33 (1996).
[24] S. Toxvaerd, J. Chem. Phys. **117**, 10303 (2002).
[25] T. L. Hill, Adv. Catal. **4**, 211 (1952).
[26] M. P. Allen and D. J. Tildesley, *Computer Simulation of Liquids* (Oxford Science Publications, Oxford, 1987).
[27] G. J. Martyna, M. E. Tuckerman, D. J. Tobias, and M. L. Klein, Mol. Phys. **87**, 1117 (1996).
[28] J. K. Johnson, J. A. Zellweg, and K. E. Gubbins, Mol. Phys. **78**, 591 (1993).
[29] V. P. Carey and A. P. Wemhoff, Int. J. Heat Mass Transfer **48**, 5431 (2005).
[30] P. Santikary, K. E. Kinney, and L. S. Bartell, J. Phys. Chem. A **102**, 10324 (1998).
[31] Y. Chusak, P. Santikary, and L. S. Bartell, J. Phys. Chem. A **103**, 5636 (1999).
[32] L. S. Bartell, J. Phys. Chem. A **106**, 10893 (2002).
[33] E. J. Jacob and L. S. Bartell, J. Phys. Chem. A **107**, 1859 (2003).
[34] D. T. Wu, Solid State Phys. **50**, 37 (1997).
[35] D. Kashchiev, Surf. Sci. **14**, 209 (1969).
[36] D. Kashchiev, J. Chem. Phys. **122**, 114506 (2005).
[37] V. P. Carey, *Liquid-Vapor Phase-Change Phenomena* (Hemisphere Publishing Corporation, United Kingdom, 1992).
[38] T. Daubert and R. Danner, *Physical and Thermodynamic Properties of Pure Chemicals: Data Complilation* (Hemisphere Publishing Corporation, United Kingdom, 1983).
[39] X. C. Zeng and D. W. Oxtoby, J. Chem. Phys. **94**, 4472 (1991).
[40] C. Xiao, D. M. Heyes, and J. G. Powles, Phys. Status Solidi B **242**, 749 (2005).
[41] E. M. Sevick, P. A. Monson, and J. M. Ottino, J. Chem. Phys. **88**, 1198 (1988).